optically detected magnetic resonance; Computational Predictions

and Experimental Results

Scott Leland Crossen

A senior thesis submitted to the faculty of
Brigham Young University
in partial fulfillment of the requirements for the degree of

Bachelor of Science

Dr. John S. Colton, Advisor

Department of Physics and Astronomy

Brigham Young University

April 2017

ABSTRACT

optically detected magnetic resonance; Computational Predictions
and Experimental Results

Scott Leland Crossen
Department of Physics and Astronomy, BYU
Bachelor of Science

electron spin resonance (ESR) is an important tool in understanding the quantum-mechanical properties of condensed matter. Its applications range from studying lattice defects in solids to studying spin coherence in qubit candidate materials used for quantum computing. When coupled with a photoluminesce measuring component, it is possible to optically record ESR information contained in the induced light. This unique form of ESR is called optically detected magnetic resonance (ODMR). In this thesis we compare experimental ODMR data with ESR predictions generated from a computational modeling system. To investigate the differences between these two methods we will study one spin-system in particular: irradiated 4H silicon carbide. This specimen will serve as the primary means to experimentally and theoretically connect the two very different forms of computational and practical ESR spectroscopy commonly used today. Methods and theory for both methods will be described and resulting spectra will be presented for comparison. Though there will always be some differences, results show that computational ESR predictions match experimental results to the same extent that the underlying Hamiltonian for that particular system is understood.

ACKNOWLEDGMENTS

Contents

List of Figures

Chapter 1

Introduction

1.1 Qualitative Description of ESR and ODMR

optically detected magnetic resonance (ODMR) is a particular form of *electron paramagnetic resonance* (EPR) which is more commonly known as *electron spin resonance* (ESR). The latter two of these terms (EPR and ESR) are synonymous; the former (ODMR) is a particular subset of ESR that utilizes a luminescence measuring technique as a means to collect ESR information. In literature, it is common to see both of these terms followed by the designation "spectroscopy" which signifies that they are tools to study properties of matter via electromagnetic radiation. Though the extent of their application has grown over the years, ESR and ODMR are most commonly used to study the spin properties of electrons and electron-holes trapped in metal lattices. They can be used to study free radicals in organic materials [**?**] and are also important in studying the local environment of lattice defects through a technique using angular-dependent ODMR [**?**]. One particular use of ODMR is the study of electron-spin coherence via a technique known as electron spin echo. This can be useful when studying what properties and conditions lead to superior state coherence for qubit candidate materials in quantum computing [**?**].

The intellectual foundation of electron spin resonance is rooted in quantum mechanics. Bound electrons in matter have discrete and quantized energy levels that govern what frequencies of light are emitted when transitions between energy levels are made. For electron systems, which are fermions and thus subject to the Pauli exclusion principle, the energy levels are two-level degenerate when bound in matter. In quantum mechanics we choose to describe this degeneracy in terms of spins: we say an electron is either "spin up" or "spin down". Each energy level can have at most two electrons of opposite spins inhabiting it (and thus the degeneracy). The spin terminology is used as to compare electrons to particles. It describes the principle of conservation of angular momentum that would be found in a classical system such as a top. In the case of an electron, the electron's spin is a description of the magnetic moment's alignment to an external magnetic field. For electrons bound in matter, the energy levels of the molecule will split in an applied magnetic field according to the zeeman effect and the spin states of the electrons can be observed — often through a photoluminescence or other fluorescence measuring technique such as what we will use here.

The zeeman effect itself is crucial in understanding the principles of ESR. In the presence of a magnetic field, populations of free electrons will form a spin-1/2 system between a lower-energy "spin-up" state and a higher-energy "spin-down" state. In matter, different half-integer values of spin states can be formed between the interactions of different energy levels with different transition selection rules. A spin-1/2 system in the presence of a magnetic field is shown in Figure 1.1. As seen here, the energy levels of the two differing spins diverge linearly for an increasing magnetic field. The difference in energy between these two levels is typically in the microwave frequency domain (for field magnitudes of a few Tesla). For higher-order systems, a given magnetic-field strength will result in a set of characteristic microwave frequencies that the electrons are most prone to emit when transitioning between quantized states. In a spin-1/2 system there will only be one frequency corresponding to the difference between the two Zeeman lines at the given field
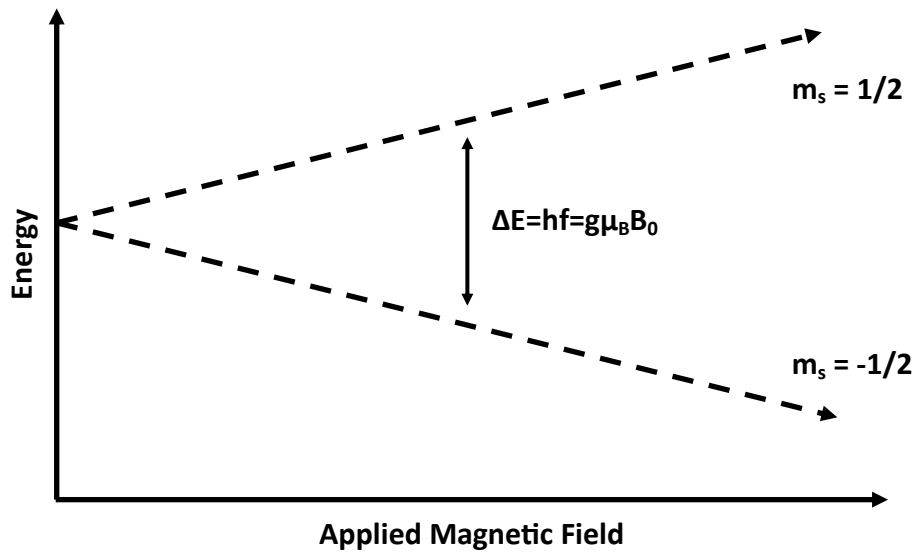
Figure 1.1 zeeman effect for a two level system showing spin ($\pm 1/2$) energy levels as a function of applied magnetic field. For arbitrary field strength the energy difference is shown as a function of μ, g, and the field strength B_0.

strength. Likewise, for a given microwave frequency, there will be a variety of magnetic field strengths which are able to transition bound electrons between states. This unique pairing between both the microwave frequency and magnetic field strength is the resonant condition upon which ESR is based on and also the means it uses to discover information about materials.

1.2 Electron Spin, Quantum Computing, and Qubits

Classical computation is based upon a binary system where the computer's register, memory, and general logical states are either in logical "true" or logical "false" states. A "true" state usually corresponds to a high voltage and a "false" state usually corresponds to a grounded voltage. A computer's bits can be in either of these two states — 1 or 0 — but not both.

A spin-1/2 system also describes a binary system between a higher energy basis state and a lower energy basis state. In this comparison, the spin-1/2 system will be measured (and the wave

function collapsed) to be in either of these two states — but not both. One important difference between the the spin-1/2 system and the classical computer bit model is that the spin system can have states that exist as a linear combination of the two basis up/down states. In accordance with quantum mechanics, this means that the spin-1/2 system can exist as a superposition between both the spin up and spin down states and has a certain probability of being measured in each. It is important to note that this superposition does not mean that the state exists as some value in between an excited state and a lower state. Rather, it exists with some value in both states simultaneously.

Because of this unique property of spin systems, they can be used as a basis for forming what is called a "quantum computer" [?]. Though it largely depends on the architecture, quantum computers can be thought of to manipulate information in a similar fashion to that of classical computers. Both have logical operators and storage bits and both are algorithmically based. Quantum computers, however, utilize this unique possibility of superposition and entanglement between states to make probabilistic calculations for many different states at the same time. This happens through quantum mechanical operations that initialize and manipulate states stored in "qubits" — the quantum computer's version of classical bits that can exist in superposition types of states.

Today, there is large emphasis within the scientific community in building viable, scalable quantum computers. The reason for this is that quantum computers offer reduced computational times for certain types of algorithms. Important to note, however, is that these machines are not necessarily more adept at common tasks, but are rather designed to carry out a few types of intense calculations in times logarithmically dependent on input for problems that would normally have a polynomial time dependence. The most notable use for quantum computers in our modern society is within the field of computer security and encryption. Quantum computers have the ability to compute prime factors via Shor's algorithm in a much faster time than traditional computers [?]. This ability would essentially render all of the current RSA encryption methods obsolete along

with everything else that relies on public/private key encryption such as bitcoin.

Although more than just spin systems can be used as the all-important qubits for quantum computing, we will focus on this type — specifically spin-1/2 systems formed from electrons — for the basis of our discussion [**?**]. As mentioned earlier, ESR is the major tool used to study the spin properties of materials. In the case of quantum computation, ESR is used to study possible qubit materials that might eventually be used in such machines. Currently, one of the major difficulties in creating quantum computers is finding materials that can form superposition states that remain coherent (and reliable) over prolonged periods of time. In order to understand what properties of materials lead to superior qubit construction and state coherence, ESR can be used in conjunction with electron spin echo experiments to study the coherence of electrons in a spin-1/2 system. Moreover, ESR can be used alone to study the spin system itself and the local environment of the defects in materials that form them. Knowledge of this important topic will serve to increase our ability to construct better qubits for use in quantum computers.

1.3   The Defect Nature of Materials

In solid-state physics, materials form crystal lattices. These structures are not perfect, however, and often have intrinsic interstitial defects [**?**]. These defects are important as they contribute to the overall spin system of the material via either electrons or holes [**?**]. For some materials, these defects can be introduced via high fluence irradiation of particles such as SiC which we will study.

1.4 Previous Work

1.4.1 Preliminary Work and Results

The work performed in this thesis references in large part the work done by Kyle Miller and Jacob Embleym, two students who worked under Dr. John Colton and have since graduated from Brigham Young University. Their work was mostly performed on the topic of electron spin coherence in proton-irradiated silicon carbide and is documented in their senior theses, both of related titles [?] [?]. This thesis, however, will not be on the same topic as the former two but will expand on one aspect used by both of these two students in their work, ODMR. In addition, both Miller and Embley used a particular species of 4H-SiC which is one of the two principal materials of investigation in this thesis.

The reference section includes a publication that Embley, Colton, Miller, myself and a few others produced on the topic of spin coherence in proton irradiated silicon carbide [?]. It has been accepted by *Physical Review B* and appeared in publication during the year 2017. This publication serves as a capstone to the work of both Embley and Miller as included in their senior theses and will serve as the context for which this thesis was produced.

In addition to the work done by Miller and Embley, an additional study was performed on a similar material of the SiC specimen which is not included in either the aforementioned theses or publication. The major difference with this project and the theses produced by Miller and Embley is the type of irradiation used on the SiC sample in question. Miller's work was primarily concerned with a 10^{14} cm^{-2} proton-irradiated sample of SiC. Embley likewise worked with a 10^{13} cm^{-2} proton-irradiated sample of SiC. In that project I worked with a 10^{17} cm^{-2} electron-irradiated sample of SiC in much the same way as used by Embley. With this additional sample, a more comprehensive analysis and additional results are presented.

1.4.2 Experimental Setup

The experimental setup used for the majority of this thesis was set up and tested by Kyle Miller and Jacob Embley. Miller initially set up all the necessary instrumentation to be used in his experiment which is detailed in his thesis. Later, Embley improved upon most of Miller's design and achieved increased precision and improved results [**?**]. The experiment used by both Embley and Miller was eventually repurposed and slightly modified for the experiment detailed in this thesis. A full summary and implementation of the experimental setup can be found in section 3.3. This section includes both the setup used by Miller and Embley as well as the components I modified for the purposes of performing this work.

1.4.3 Samples and Collaborative Efforts

The work done for this thesis was done in collaboration with two groups of people. Firstly, the silicon carbide samples used were produced and partially characterized by Dr. Sam Carter of the Naval Research Lab [**?**]. These samples were irradiated with different fluences of particles in order to introduce different concentrations of defects into the material. It was Carter's work that ultimately led us to obtain such high quality samples for optical characterization and electron spin resonance studies.

1.4.4 Preliminary Results of Experimental ODMR

This thesis is based around one primary material, SiC, which was previously characterized for ODMR.

Dr. Sam Carter of the Naval Research Lab provided the SiC samples we used. According to his characterization, the silicon vacancies in silicon carbide form a spin-3/2. This system also has a zero-field splitting effect which creates an energy difference between the positive and negative

spin states even with no external field. (+3/2, +1/2 with -3/2, -1/2).
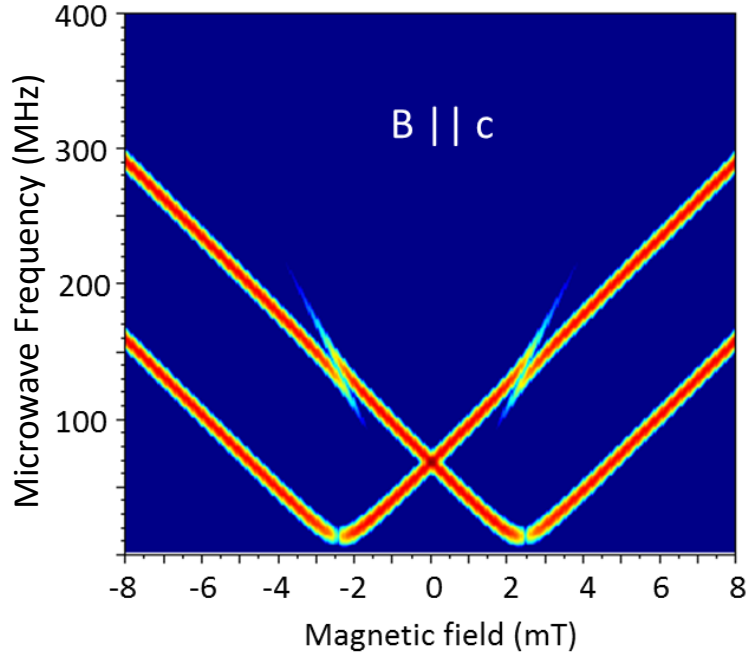
Figure 1.2 The relationship between magnetic field strength and microwave frequency for 4H-SiC, a spin-3/2 system. Color Brightness indicate resonant conditions. Notice the linear dependence between both microwave energy and field strength.

In addition Dr. Carter also provided preliminary ODMR results performed at low field strengths of around 31 mT [?]. The results of his measurements are found in Figure 1.3 and show the transitions between different spin states which will be more fully developed in section 3.1.1. Moreover, Carter also provided angular dependent measurements of resonant conditions between magnetic field strength and microwave frequency. As mentioned in section 1.1, for a given magnetic field strength there will exist different resonant frequencies depending on the spin system in question. In addition, these characteristic frequencies will have associated linewidths that describe what range of frequencies the resonance is centered around and how wide it is. For the case of a spin-3/2 system as found in 4H-SiC, the relationship is best represented by Figure 1.2 which is a plot produced by Dr. Carter for the samples used in this project [?].
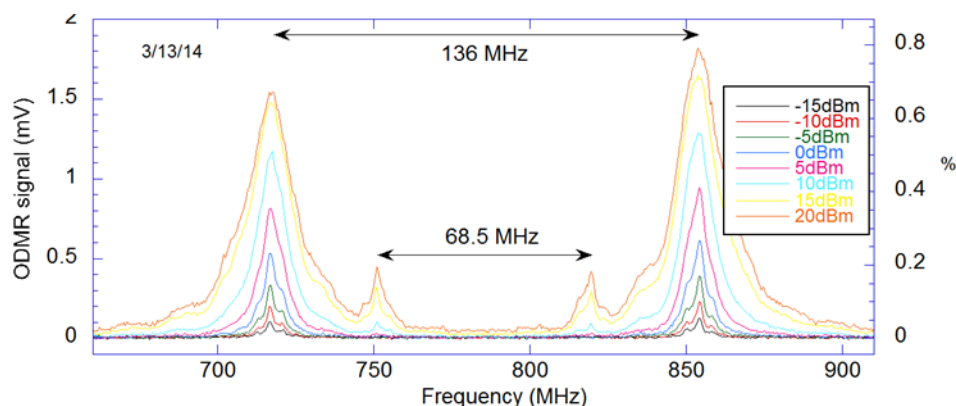
Figure 1.3 The preliminary ODMR data for proton irradiated silicon carbide in a constant magnetic field of 28 mT. The plot shows resonant paramagnetic conditions at 718 MHz and 857 MHz where the absorption is greatest.

1.4.5 *EasySpin* Computational Modeling System

EasySpin [**?**] is a library for MATLAB designed to computationally model ESR data. The majority of computational work for this thesis was done using this program which was provided free of charge through the program's website. Though most of the necessary functions to model ESR data were included in the *EasySpin* library, I still found it necessary to create custom definitions in addition to what was already supplied.

1.5   Overview of Thesis

The purpose of this thesis is to describe in detail the methods and procedures behind experimental and theoretical ESR and to answer the question as to how both experimental and theoretical methods compare to each other. By so doing we will also introduce the fundamental theory behind ESR and computational modeling packages such as *EasySpin*. In addition, we will also discuss the experimental frameworks and setups necessary for collecting ODMR information from materials. This analysis will not be comprehensive but is rather purposed as an introduction into the

techniques used in the field. As such, we will restrict our analysis to only solid-state ESR and ODMR.

We will use one main material for this thesis: SiC. This material will be valuable in our understanding of lattice defect contribution towards ODMR results. In addition, we will primarily use this material as a control to compare the experimental data with respective computational predictions. It will be through this material that we will ultimately show the similarity between experimental results and theoretical predictions.

In the end, this thesis will conclude that computational modeling is accurate to the same degree the spin system is understood. In other words: the level of precision that computational modeling can present is restricted by how much information is known about the Hamiltonian for that given system.

1.6   Explanatory Notes and Background Information

The content of this thesis will use the term *ESR* when referring to the general theory and mathematical model of electron spin resonance and will use the term *ODMR* when referring to the experimental methods used for collecting ESR information. As mentioned earlier, ODMR is a specific type of ESR that is ultimately used to collect the same information through a fluorescence technique. Because we have implemented an ODMR-type experiment in our lab we will use this term for descriptive accuracy when referring to our experimental application.

By way of information, the work done for this thesis was performed using MATLAB R2016b (version 9.1) and *EasySpin* version 5.1.9 . It will be assumed that the reader is proficient in basic MATLAB or C constructs and is at least familiar with data types and terms such as "struct", "parameter" and "field" as related to computer programming.

All plots and figures were created using a combination of Mathematica version 10.4 and Origin

version 7.5.

In addition, pertinent git repositories will be hosted online via GitHub for all code developed for this project. The LabVIEW suite used for data acquisition can be found at the permanent URL https://github.com/coltonlab/LabVIEW-programs. The programs developed on top of the *EasySpin* library that were used for theoretical modeling can be found along with this thesis at https://github.com/scottcrossen/SeniorThesis.

Chapter 2

Computational Model and Theory

2.1 Mathematical Theory

As mentioned in the Introduction, spin systems and electron spin resonance (ESR) are best understood in terms of interaction Hamiltonians. "Hamiltonians" in this context are quantum mechanical operators (as opposed to the classical mechanical version) that act on energy states and form specific eigensystems with defined energy eigenvalues. For example, in the zeeman effect there exists a Hamiltonian that when diagonlized gives the energy-splitting for a given magnetic field in terms of its eigensystem. Since ESR spectroscopy measures the resonant conditions between energy-levels and magnetic field strength, it is necessary to calculate the field-dependent Hamiltonian for each system before we can calculate the theoretical ESR spectrum.

Thankfully, the general Hamiltonian for atoms in a magnetic field is commonly known [**?**] [**?**]. In this case, the interaction energy of an atom in a constant magnetic field is given by the overall spin Hamiltonian $\mathscr{H}_{\text{tot}}$ [**?**]

$$\mathscr{H}_{\text{tot}} = \mathscr{H}_{\text{elect}} + \mathscr{H}_{\text{cf}} + \mathscr{H}_{\text{LS}} + \mathscr{H}_{\text{SS}} + \mathscr{H}_{\text{Zee}} + \mathscr{H}_{\text{hfs}} + \mathscr{H}_{\text{Q}} + \mathscr{H}_{\text{N}}$$

where $\mathscr{H}_{\text{elect}}$ is the electronic energy, $\mathscr{H}_{\text{cf}}$ is the crystal field energy, $\mathscr{H}_{\text{LS}} = \lambda \mathbf{L} \cdot \mathbf{S}$ is the spin-

orbit interaction, $\mathscr{H}_{SS} = D\left[S_z^2 - \frac{1}{3}S(S+1)\right]$ is the spin-spin interaction, $\mathscr{H}_{Zee} = \beta\mathbf{H}\cdot(\mathbf{L}+\mathbf{S})$ is the Zeeman interaction energy, $\mathscr{H}_{hfs} = (A_x S_x I_x + A_y S_y I_y + A_z S_z I_z)$ is the hyperfine structure, $\mathscr{H}_Q$ is the quadrupole energy, and $\mathscr{H}_N = \gamma\beta_N\mathbf{H}\cdot\mathbf{I}$ is the nuclear spin energy. All of these components are defined in terms of the spin angular momentum operator $\mathbf{S}$, the orbital angular momentum operator $\mathbf{L}$, the Nuclear Spin Operator $\mathbf{I}$, the Bohr magneton β, the spin-orbit coupling constant λ, the hyperfine coupling constant A, the nuclear gyromagnetic ratio γ, and the zero-field splitting constant D.

Some terms in the Hamiltonian dominate the system and can be focused on individually. The most important term is the Zeeman interaction energy. For the high-field limit that we will be working with, the Zeeman interaction dominates all other perturbations. This affects the system by splitting energy levels linearly with increasing magnetic field. Though there are a few other constants involved in the calculation of the Zeeman Hamiltonian, the main parameter it requires is the all-important g-tensor which can be extracted from the Hamiltonian given above. We can show this process explicitly by writing the form of the Zeeman interaction as $\mathscr{H}_{Zee} = \beta\mathbf{H}\cdot(\mathbf{L}+\mathbf{S})$. Simplifying this for a constant field in one direction gives $\mathscr{H}_{Zee} = \frac{\mu_B\mathbf{B}}{\hbar}\cdot(g_l L_z + g_e S_z)$. Now if we solve specifically for the Zeeman corrections to individual terms ΔE_{Zee} we get $\Delta E_{Zee} = \frac{\mu_B\mathbf{B}}{\hbar}\cdot(g_l m_l\hbar + g_e m_s\hbar)$ where m_l and m_s are orbital and spin quantum numbers respectively. In the coupled basis we typically represent this in terms of one g-factor g and one quantum-number m: $\Delta E_{Zee} = g\mu_B\mathbf{B}m$. The resulting g-tensor is specific to individual materials and simplifies to a factor for symmetric lattice conditions. It describes the spreading of the different spin energy levels in the magnetic field and it is ultimately through this Zeeman effect that we are able to see resonant conditions between magnetic field strength and microwave frequency.

Once the Hamiltonian is known for the system, the ESR spectrum can be computationally predicted. A variety of methods are available to go from the basic Hamiltonian components to the finished ESR plot. The most notable is a software suite called *EasySpin* [**?**], which vastly simplifies

the amount of calculations and explicit Hamiltonian definitions that the investigator has to make.

2.2   *EasySpin* Interaction Modeling System

The purpose of this thesis is to show the unique methodologies of both computational and experimental ESR. As for the former of these two, the most common tool used to computationally model ESR is known as *EasySpin* [**?**]. This package is built as an open library on top of the MATLAB program and serves to add functionality to the already-useful suite of functions that components within MATLAB.

2.2.1   The *EasySpin* Struct Definition

The core utility of the *EasySpin* package is the definition used in the spin system. The *EasySpin* library is built around the idea of a struct (a term describing a publicly-scoped group of fields) to define all necessary components of the system being studied. In fact, most methods in the *EasySpin* library usually require just a struct of this type as the sole parameter in the function declaration.

```
Sys.S = 1/2;
Sys.g = 2.017;
Sys.lw = 1;

Exp.mwFreq = 9.2;   % GHz
Exp.Range = [320 330]; % mT
```

Figure 2.1 An example declaration of the basic *EasySpin* struct used in defining the spin system. In this example, "Sys" represents an arbitrary name for the struct, ".S" is the spin parity, ".g" is the g-factor, '.lw' is the ESR line-width, ".mwFreq" is the position of the microwave frequency being probed, and ".Range" is the range of the magnetic field being scanned.

The struct represents the spin system and is usually defined by the user to the extent that the system is known. Though there are many optional parameters that can be included in the struct,

the most rudimentary spin system needs to include a ".S" parameter representing either a list or a value for the half-integer value of spin being worked with as well as a ".g" parameter to represent the g-factor of that material in solid-state ESR. The g-factor could be either a list or a single value depending on the crystal type being investigated. After these two parameters are defined, the system can then be passed to any other functions for analysis and plotting. Figure 2.1 shows an example of what this basic definition might look like in MATLAB.

2.2.2 Basic Class Structure

The term "class" is used loosely in this context. Unlike most languages, MATLAB (and thus *EasySpin*) is based on plain C and is thus not really object oriented. However, unlike C, basic class definitions have been added to MATLAB though they aren't commonly used. *EasySpin* uses a series of ".m" files that represent different abstractions of the overall modeling system that may or may not be implemented in the form of classes. For this thesis, I will use the term "class" to refer to any modular component of the provided *EasySpin* library.

The most notable classes that are supplied with the library are the core plotting functions for ESR spectra [**?**]. These include such names as "garlic" for cw isotropic ESR and "pepper" for solid state CW ESR (which I will use). Table 2.1 shows the full list of possible plotting functions supplied in the library. Other functions supplied in *Easyspin* are mostly related to data import/export, data analysis, and system optimization.

Table 2.1 List of possible *EasySpin* plotting functions. '*pepper*' is the main function that will be used in this thesis.

Function	Description
garlic	cw EPR, isotropic and fast motion
chili	cw EPR, slow motion
pepper	cw EPR, solid state
salt	ENDOR, solid state
saffron	pulse EPR/ENDOR, solid state
curry	SQUID magnetometry
blochsteady	Bloch equations, steady-state
pulse	Shaped pulses
esfit	least-squares fitting

In addition to the classes supplied in the *EasySpin* library, I have also built a few of my own for better visualization of spin systems. One such class (which is included in the online repository cited in the introduction) is called "zeeman.m". This program plots the field splitting of the Zeeman interactions in the spin system vs increasing magnetic field. Another class I implemented builds upon this one and is called "animate.m". This plots the Zeeman diagram and then animates the plot by drawing the resonant magnetic field differences for a given microwave frequency. Again, all of these additional classes are included in an online repository linked to in the introduction of this thesis.

2.3   Selecting Hamiltonian Arguments

In order to do emulate ESR spectrum via *EasySpin*, the Hamiltonian for the materials needs to be understood to the fullest possible extent.

2.3.1 ZnO Nanowires

As a demonstration of how to use *EasySpin*, I have recreated the results given by J. E. Stehr in his publication regarding the resonant properties of zinc oxide nanowires [**?**]. In this paper, the author Stehr models the ESR spectrum using g-tensor and spin-values given for each defect center of ZnO nanowires. This data is summarized in Table 2.2. Stehr used the *EasySpin* modeling system to show the predicted ESR spectrum resulting from the V_{Zn}^-, V_{Zn}/Zn_i, and D^* defect center contributions. He modeled each Hamiltonian separately using *EasySpin* and then combined the results with MATLAB. Figure 2.2 shows the published plots.

Table 2.2 Summary of the spin Hamiltonian parameters for the various defect centers of ZnO nanowires given by J. E. Stehr et al [**?**]. The spin-parity and diagonalized g-tensor values are given for each defect center. For the non-axial centers, φ is the angle between the z and c axis.

Center	S	Axial		Nonaxial			φ (deg)
		$g_\perp$	$g_\parallel$	g_{xx}	g_{yy}	g_{zz}	
V_{Zn}^-	1/2	2.0193	2.0024	2.0173	2.0183	2.0028	110.75
Z	1/2	2.006	2.020				20
V_{Zn}/Zn_i	1			1.9888	1.9893	1.9815	110.75
Zn_i^+	1/2	1.9595	1.9605				0
D^*	1/2	1.9595	1.9605				0

However, one thing Stehr did not include was the ESR line-width parameters and derivations he used when constructing the spin system via EasySpin. As a verification for the process he used, I have included a reconstruction of the same ESR spectrum that was included in his publication. Through comparison I found that the line-width parameters used by Stehr were 1, 5, and 2 mT for V_{Zn}^-, V_{Zn}/Zn_i, and D^* respectively. Though it is unknown as to how he arrived at these values, it is likely that he compared the theoretical model to the experimental data until a reasonable fit was

achieved. In Figure 2.3 and 2.4 I give the re-creation of the spectrum and the code used to generate
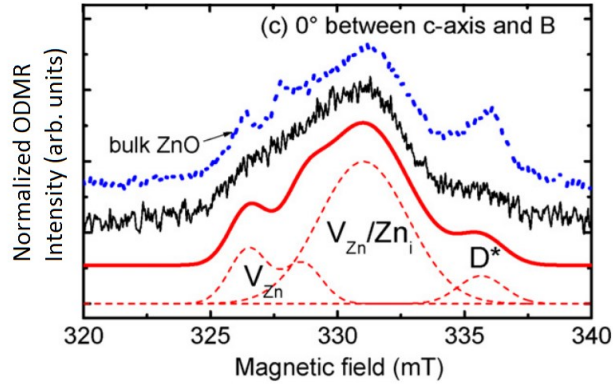
the spin system that Stehr used [**?**].

Figure 2.2 The ESR spectrum presented by Stehr et al for ZnO nanowires [**?**]. The results of computational modeling using *EasySpin* are shown in dashed-red (individual) and solid-red (total). The black line represents actual data from the sample and the blue line is included for comparison to the bulk species.
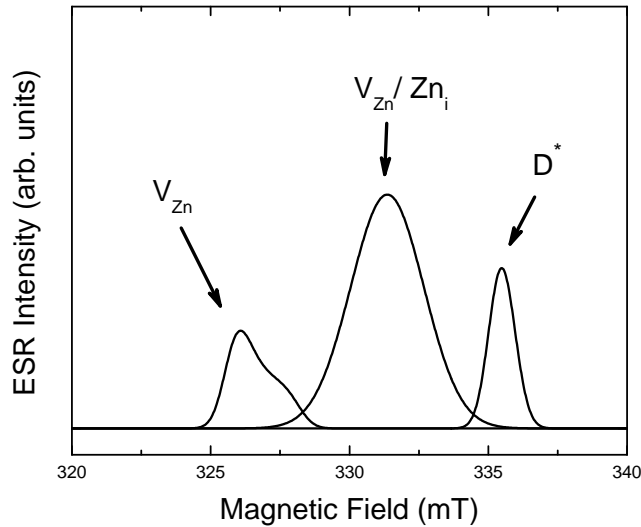

Figure 2.3 The re-creation of the plots given by Stehr et al. for the ZnO nanowire ESR spectrum. All three defect centers are included as in the original figure.

```
Sys1.S = 1/2;
Sys1.g = [2.0173, 2.0183, 2.0028];
Sys1.gFrame=[0 0 110.75];
Sys1.lw = 1;

Sys2.S = 1/2;
Sys2.gFrame=[0 0 20];
Sys2.g = [2.006 2.020];

Sys3.S = 1;
Sys3.g = [1.988, 1.9815, 1.9815];
Sys3.gFrame=[0 0 110.75];
Sys3.lw = 3;

Sys4.S = 1/2;
Sys4.g = [1.9595 1.9605];

Sys5.S = 1/2;
Sys5.g = [1.9605 1.9565];
Sys5.lw = 1;

Exp.mwFreq = 9.2;   % GHz
Exp.Range = [320 340]; % mT
Exp.Harmonic=0;
```

Figure 2.4 The *EasySpin* struct definition used in the creation of the plots given by Stehr et al.

2.3.2   Irradiated 4H-SiC

In order to computationally model the ESR spectrum for SiC, we first need to first construct the Hamiltonian for the system. In the following paragraphs I will detail the major components that make up the spin Hamiltonian for SiC. I have also included the pertinent code to represent this system in terms of the *EasySpin* struct definition in Figure 2.6.

SiC is a commonly known to be a spin-3/2 system with two major ESR peaks in its spectrum [**?**]. The parameter ".S" given for the *EasySpin* system is simply 3/2. Moreover, as mentioned previously, SiC has one major defect of interest: the silicon divacancy [**?**] [**?**] in its lattice structure. The g-factor for this defect is given as a rhomboidal two-termed g-factor [$g_{xx} = g_{yy}$, g_{zz}] of almost exactly 2 [**?**]. This is listed as the ".g" parameter in the struct definition.

The linewidths are relatively narrow for specimens related to SiC. By comparison to experiment
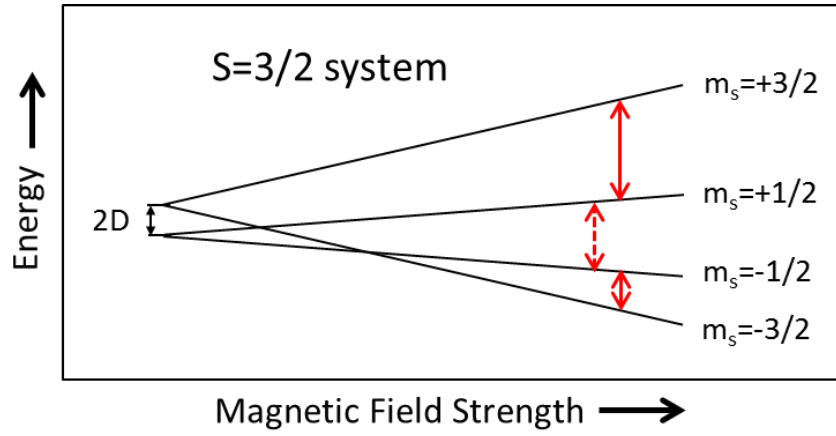
Figure 2.5 A diagram showing the energy-levels of the spin-3/2 system inherent in 4H-SiC for the high-field limit. Allowed transitions are shown with solid colored arrows. Disallowed transitions are shown with dashed arrows

```
Sys.S = 3/2;
Sys.g = 2.008;
%Sys.A = ??;
%Sys.Nucs = '29Si';
Sys.D = 34;
Sys.lwpp = [8 1];
Sys.DStrain=5;

Exp.Field = 370.78; % mT
Exp.mwRange=[10.2 10.6]; % GHz
Exp.nPoints=1024;
Exp.Harmonic=0;
Exp.Temperature=298;
Exp.CrystalOrientation = [0 0 0]*pi/180;

Opt.Transitions=[1 2; 3 4];
```

Figure 2.6 The representation of the known parameters included in the *EasySpin* struct definition for analysis of 4H-SiC

we have found that the full-width-half-maximum value of the line-widths is close to unity. Using *EasySpin* this means that the ".lw" parameter should be set to around 1. For the code provided in Figure 2.6 I have used a more-advanced form of Lorentzian line-broadening to achieve this result.

One interesting property of this material is that it exhibits a zero-field splitting which divides the $+3/2$ and $+1/2$ from the $-1/2$ and $-3/2$ states even when there is no external magnetic field. Our collaborater Dr. Sam Carter measured this parameter to be on the order of ".D= 70" MHz at the zero-field marking [**?**]. For the struct definition in Figure 2.6 we have used half of this value in accordance with the different definition of the term as used by *EasySpin*.

Moreover, only certain transitions are allowed in the SiC spin-3/2 system. Though other transitions can happen, they are unlikely and also undetectable because of the mechanism used by ODMR. For SiC the allowed transitions are between the energy levels of +3/2 to +1/2 and -3/2 to -1/2 [**?**]. To account for this effect in our *EasySpin* code we will use an optional parameter called ".Transitions" which we will set to only allow those transitions.

Though it is not readily apparent, SiC also exhibits hyperfine splitting in its major ESR peaks. To observe this splitting, two terms can be added to the spin-system: ".A" and '.Nucs'. For SiC these two parameters take on the value of "-120" and "29Si" respectively. However, in our example these terms are insignificant and therefore not included. In Figure 2.6 I have commented out two lines of code to reflect this fact.

Chapter 3

Experimental Methods

The work done for this thesis uses both computational and experimental components in describing ESR. We have described the process of theoretical/computational ESR in the last chapter. In this chapter we will describe the experimental methods of ESR which we call ODMR due to its optical-coupling of information gathering. This chapter is primarily concerned with detailing the experimental methods implemented in typical ODMR setups. We will first begin with a qualitative description of the material we studied (SiC).

3.1   Sample Preparation

3.1.1   Preparation of Silicon Carbide Samples

Three different samples of 4H-SiC were provided to us by our collaborator Dr. Sam Carter of the Naval Research lab. Each sample was prepared with a different irradiation fluence to introduce silicon defects into the lattice. The first sample that we tested was irradiated with 2 MeV protons at a fluence of 10^{14} cm^{-2}. The second sample was similarly irradiated with 2 MeV protons but at a fluence of 10^{12} cm^{-2}. The final sample was an electron-irradiated sample produced with a

fluence of 10^{17} cm^{-2}. The different strengths of irradiation in each sample is presumed to change the concentration of vacancy defects formed within the sample.
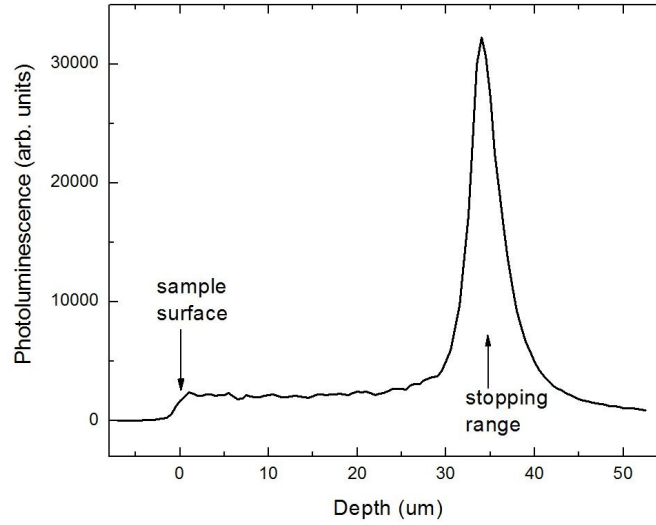

Figure 3.1 Depth-dependent photoluminescence of the 10^{12} cm^2 sample at at major PL peak. The large peak at 34 μm indicates the stopping position of the protons. The spatial resolution was 1 μm.

A higher irradiation fluence typically produces a higher concentration of defects. Figure 3.1 shows the depth stopping depth of irradiated protons in a 10^{12} cm^{-2} sample given to us by our collaborator Dr. Sam Carter [**?**]. This plot of stopping depth should roughly correspond to the location of defects in the sample. From the SRIM calculations, Dr. Carter predicted that the stopping distance of the ions would be at about 44 μm from the sample's surface. However, further photoluminescence studies showed the concentrations to be closer to about 32 μm rather than 44 μm.

Though we recorded the ODMR spectra for all the SiC samples, there was no real difference between any of them. By way of information, however, the data reported in this thesis corresponds to the the10^{12} cm^{-2} proton irradiated sample
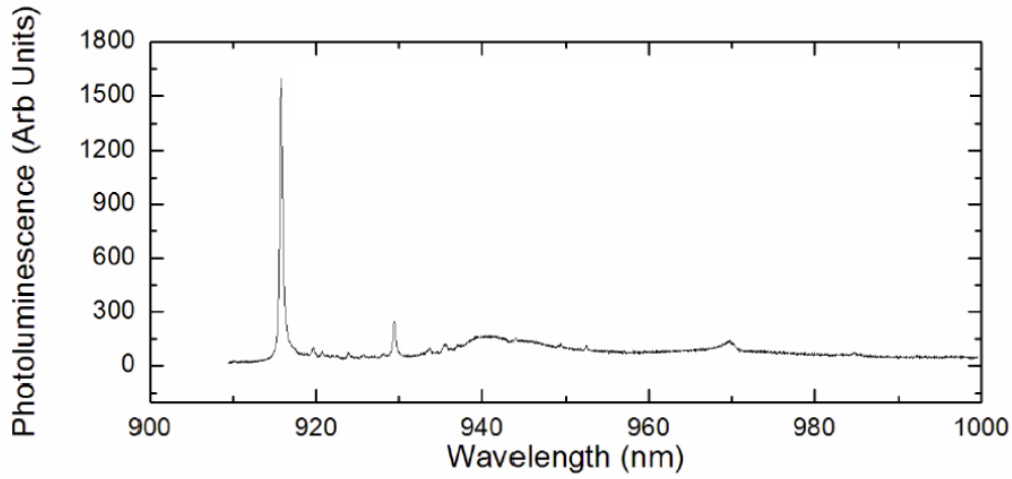
Figure 3.2 Photoluminence plot showing PL strength vs. wavelength in SiC. The peak near 915 nm is the primary peak of interest as it represents the V2 silicon vacancy defect.

3.1.2 Photoluminescence Data

As mentioned earlier, ODMR is a particular type of ESR. The major difference is that ODMR uses a double-resonance technique combining the resonant effects from ESR with the optical methods of Photoluminescence to collect ESR data. Because of this, our SiC sample had to exhibit specific conditions in it's photoluminescence spectrum in order for the absorption of the microwave frequencies to be measured by our detectors. Figure 3.2 shows the photoluminescence spectra of SiC with the major peak of interest shown at 917 nm.

3.2 Experiment Background

The experiments performed in this thesis were performed in tandem with another study involving electron spin coherence in silicon carbide. The majority of the equipment used in the spin-studies project was alos used directly for collecting data for this thesis. Because of this, section 3.3 only summarizes the more important elements and also those aspects of the experiment that significantly
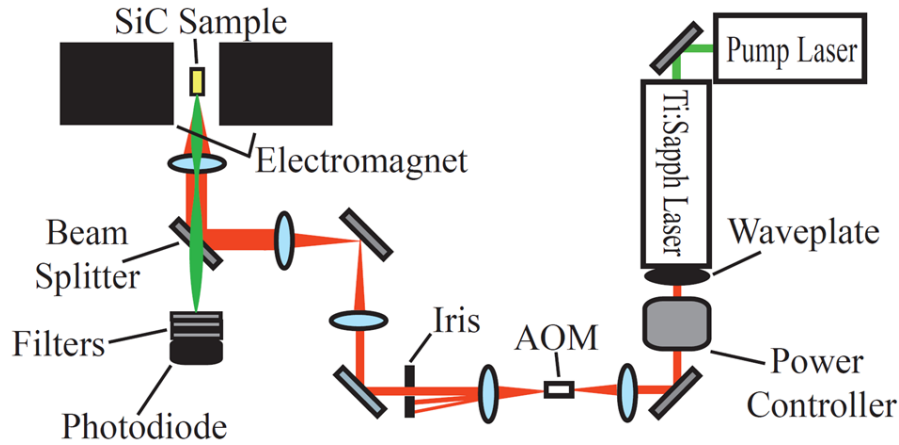
Figure 3.3 The diagram showing the necessary (labeled) components and arrangement for the ODMR experiment. A full description of each element is included in section 3.3.

deviate from previous projects. For a more detailed description of the experiment please reference to Jacob Embley's undergraduate senior thesis. [**?**]

3.3 Experiment Setup

The overall setup used in this experiment is shown in Figure 3.3. The basic components necessary to collect ODMR data are: A laser to stimulate photoluminescence, a constant magnetic field, and an adjustable microwave generator to transition spins between energy levels. For our purposes the sample was mounted in a cryostat which kept it at a constant temperature for consistency in the experiment. These components are described in detail in the next section.

3.3.1 Temperature Controller and Static Magnetic Field

All samples that we studied were held at constant temperature and magnetic field. A nonmagnetic CryoIndustries cryostat was used to maintain constant temperature on the sample throughout the duration of the experiments. A turbopump was used in addition to the cryostat to keep the pressure around 10^{-5} mbar. A PID CryoCon controller was used as the heating element in the chamber.

When used in combination with the cryostat, any temperature between 8 K and 300 K could be achieved. Many different temperatures of ODMR were recorded for the samples between these two temperatures.

Most ESR-type experiments hold microwave frequency constant and sweep magnetic field strength, but for our purposes it was easier to do this in the reverse manner. As our data shows, the results can be interpreted the same way for either method. An external static magnetic field of 0.37 T was applied constantly throughout the experiment. A large iron-core electromagnet was powered using a Magna-Power Electronics TS Series IV power supply. A Lakeshore DSP 750 gaussmeter was used as a PID controller to make fine adjustments to the magnetic field so that it stayed constant at 0.37 T.

3.3.2 Laser and Optics

In order for photoluminescence to be measured off the sample, a laser was used to stimulate emission in the sample. The laser used for this experiment was a 3900 S Ti:Sapph laser tuned to 870 nm and pumped by a 532 nm solid diode laser. The Ti:Sapph was focused to around 50 micrometers and controlled by a Brockton Electro-Optics Corp BEOC laser power controller. The laser was chopped with a NEOS Technology 15210 acousto-optic modulator (AOM) and paired with a Stanford Research System lock-in amplifier recording filtered light from a photodiode.

3.3.3 Microwave Generation and Amplification

Microwaves induce transitions between the Zeeman energy levels and are the fundamental variable modulated to retrieve ODMR data. The microwaves used for this experiment were produced using an Agilent Technologies E8257D microwave generator set at 10.4855 GHz at 0 dBm. A 20T4G18 traveling wave tube microwave amplifier increased the power of the microwaves up to about 40 dBM. The microwaves were then fed to a coupling loop placed next to the sample within

the cryostat.

3.3.4   Software Controller Interfaces and Data Recording

All experiments were conducted using a LabVIEW suite of programs designed to easily gather and record ODMR data. For our experiment, the LabVIEW suite controlled the microwave and laser modulating so that both could be referenced with a lock-in amplifier as necessary. The microwave generator and lock-in amplifier were interfaced using a GPIB addressing bus implemented as a separate class instantiation in the main LabVIEW program. The instrument classes were all designed to run in parallel to the main scanning software for better experimental isolation. The generic scanner object was built to handle an abstracted object implementing a "scannable" interface and another object implementing a "readable" interface. The scanner was built robustly enough to handle any combination of instrumentation that inherits from these two interfaces. It gives directives to the "scannable" object while also recording data from the "readable" object at the same time. A beta version of the program is linked-to in the introduction of this thesis and represents the ongoing work of myself, Ryan Peterson, Kyle Miller, Phil White, John Colton, and others.

In addition to the main LabVIEW suite of programs used, an additional PID-controller VI was built to run on its own computational thread. This was used to handle the magnetic field strength incident on our sample and make minor adjustments to the power-supply for the magnet according to measurements read off of the gaussmeter inserted into the field.

The overall program accepts as input a range of microwave frequencies and then records the absorption from the sample representing the ODMR. After this data was recorded, a graphing software known as *Origin* was used to produce plots from the raw data. No other data analysis was needed apart from the straight reproduction of the raw data into readable plots. The concluding chapter shows these results.

Chapter 4

Results

This chapter presents the ESR spectrum of SiC for both computational and experimental methods. The results of these two methods are then compared and contrasted and their strengths analyzed.

4.1   Computational Predictions

Using computational methods via spin Hamiltonian analysis with *EasySpin* we were able to recover the characteristic ESR spectrum shown in Figure 4.1. The figure shows resonant peaks at 10.35 GHz and 10.47 GHz for a field strength of $370.78mT$. Though there are only two major peaks, if we had defined our Hamiltonian further we may have been able to see smaller perturbation effects such as the fine and hyperfine structures.
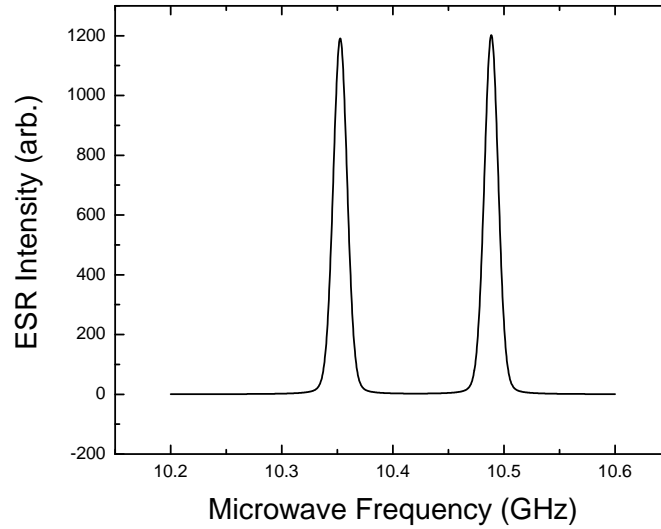
Figure 4.1 The uncorrected computational model for the ESR spectrum of 4H-SiC plotted for a magnetic field strength of B=370.78 mT. The plot shows the the relation between microwave frequency absorption for a static magnetic field strength.

4.2 Experimental Results

We successfully collected data showing the ODMR spectra for SiC. This data is shown in Figure 4.2. The same trend is seen in this data as is shown in the previous predictions. Namely, there are resonant peaks at 10.35 GHz and 10.47 GHz for a field strength of 370.78 mT. Also visible in this figure is a minor splitting of each peak visible at the very top of each spectral line. This is attributed to higher-order structures resulting from the perturbation of the material's energy levels.
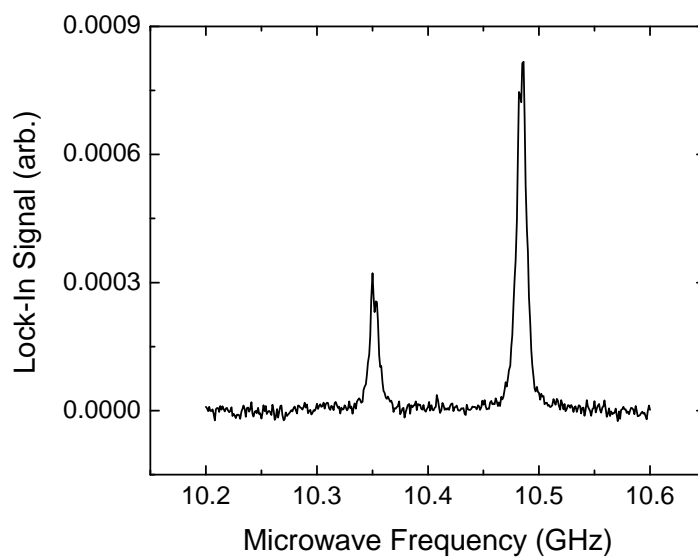
Figure 4.2 The experimental ODMR results for 4H-SiC for a magnetic field strength of B=370.78 mT. Like the computational predictions, this plot also shows the the relation between microwave frequency absorption for a static magnetic field strength.
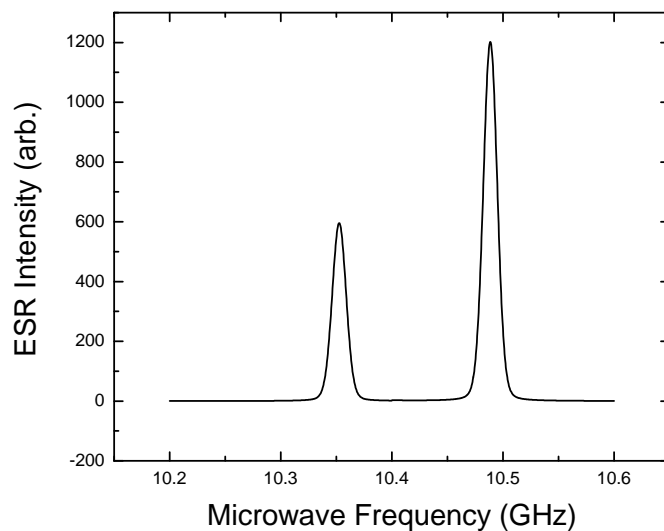

Figure 4.3 The manually-corrected computational model for the ESR spectrum of 4H-SiC plotted for a magnetic field strength of B=370.78 mT. In this plot the first minor peak has been corrected to reflect unaccounted Hamiltonian parameters

4.3   Data Analysis

The main expectation of the two different ESR methods is that both will produce spectral peaks at the same resonant microwave/magnetic field pairings. Moreover, it is also expected that the relative heights of each spectral peak are the same when compared between plots. The data presented in the previous sections corroborate at least the first of these two conditions. There is still is some differences between the two methods beyond these conditions. For example, the experimental ODMR shows a higher noise-floor than the computational method. It's easier to predict cleaner spectras when the only uncertainty is that of machine precision and not environmental effects.

It is expected (and actually acceptable) that there will be some variations in the results obtained between the two methods used to recover ESR information from materials. The most notable difference between the two methods is seen in the width of each spectral peak within the plots. Though it is similar, there is a quantitative difference between the two plots. Theoretically the probability of transitioning between microwave-levels in the samples should reach a delta-function limit centered at the resonant frequency for that given field strength. However, in practice this does not happen due to inhomogeneities within the material itself. ESR peaks are instead shown to have finite widths in the magnetic-field domain. Though the experimental results are easily reproducible given the same parameters, different investigations may find different values of width depending on how the silicon carbide samples were produced. It is therefore not hard to explain why the computational predictions that were obtained for ESR do not always match the experimental results when there is such discrepancy among experimental procedures themselves. For our purposes a spectral line-width parameter was used to best match the experimental results that we obtained.

One of the major problems with modeling ESR spectra is that so many minor experimental conditions can fundamentally change the spin-system being studied and thus change what the resultant spectrum looks like when being modeled. As mentioned, computational models are only effective to the extent that the Hamiltonian for the system is understood. For the case of silicon

carbide, there is still many details about the material that are not well understood — or simply not known — about the system. For example, there is still a lot of speculation and ignorance regarding the exact effect of the nuclear-spin interaction, the effects of the ODMR PL-mechanism, and the effects of the inhomegenous distribution of defects in the sample. To account for this, Figure 4.3 shows the data from Figure 4.1 except with the spectral peaks treated separately in the Hamiltonian such that the relative peak-heights can be adjusted appropriately to match the experimental results.

4.4   Conclusion

The primary conclusion of this thesis is that though there are some differences between the two methods, the results show that computational ESR predictions match experimental results to the same extent that the underlying Hamiltonian for that particular system is understood. In other words: the level of precision that computational modeling can present is restricted by how much information is known about the Hamiltonian for that given system. Furthermore, there will always be some ambiguity between ODMR results and predictions due to practical considerations such as noise and ESR line-widths. Overall however, computational methods are good approximations of actual ESR results.